Electronic shell effects in triaxially deformed metal clusters: A systematic interpretation of experimental observations

C. Yannouleas and Uzi Landman
School of Physics, Georgia Institute of Technology, Atlanta, Georgia 30332-0430
(Received 26 September 1994)

We develop and apply a semiempirical shell-correction method to calculate the binding energies of open-shell, neutral and charged, simple-metal clusters, which can be modeled as triaxially deformed jellium droplets. Systematics of ground-state properties of clusters with sizes up to 100 atoms, such as ionization potentials and electron affinities, are studied and compared to available experimental measurements on sodium, potassium, and copper clusters. We also report on systematics of the energetics of fission channels for doubly charged cationic and anionic species, as well as the energetics of monomer and dimer separation channels, and compare them to experimental data. Pertaining to characteristic patterns as a function of cluster size in the above quantities, triaxial shell effects exhibit a rich structure, yielding overall substantial improvement in the agreement between theory and experiment. In particular, we show that the lifting of the degeneracies in the electron spectra via cluster triaxial-shape deformations underlies the appearance of odd-even alternations in such patterns. Furthermore, our analysis of ground-state properties can lead to unambiguous assignments of equilibrium cluster shapes, as well as shape isomers.

I. INTRODUCTION

Early in the study of alkali-metal clusters, it was recognized that their ground-state properties portray manifestations of electronic shell effects.[1–4] An important step toward understanding these effects has been achieved by modeling the clusters as spherical-jellium droplets, where the ionic structure of the cluster was modeled by a continuous positive charge distribution having a sharp-step spherical profile, and the electrons were treated using density functional theory in the local-density approximation[2,4–6] (LDA). However, while analyses restricted to consideration of spherical shapes have been able to account for the main discontinuities observed at cluster magic-number sizes (associated with the filling of degenerate levels of valence electronic states which are grouped into a major shell), the results obtained by such spherical models, pertaining to the overall behavior of cluster properties versus size, are not in satisfactory agreement with the experimental data.[3] For example, for ionization potentials, the spherical jellium yields typical sawtoothed curves, which lack fine structure between major shells, a feature that is prominent in the data. In addition, each arc of the sawtooth rises steeply above the data before falling sharply at the next discontinuity associated with a major-shell closure. This behavior contrasts with the observed ionization-potential (IP) curves, which remain rather flat between magic species, exhibiting a staircase profile.

The merit of the early spherical-jellium model of clusters derives from the recognition of the importance of level bunching in the single-particle spectra of finite systems. The degree of level bunching is related to the degeneracies imposed by the symmetry of the systems. As is well known in various branches of physics (i.e., atomic, molecular, and nuclear physics), the high degree of degeneracy pertaining to spherical symmetry is associated with closed-shell systems. Open-shell systems, on the other hand, lower their energy via various symmetry breaking mechanisms which result in diminished degeneracies. In atomic systems, the spherical symmetry of the nuclear central-field potential felt by the electrons is broken by the repulsive interelectron Coulomb interaction leading to a level-filling scheme favoring high-spin multiplicity according to Hund's rule.[7] In molecules (and solids), the lifting of orbital degeneracies occurring through structural distortions is known as the Jahn-Teller effect.[8] In open-shell nuclei, energy stabilization occurs via shape deformations[9–13] (a mechanism that may be thought of as akin to the Jahn-Teller effect).

For open-shell clusters, in analogy with atomic nuclei, it has been suggested that consideration of quadrupole shape deformations could lead to lifting of the spherical degeneracy and to an improvement in the agreement between theory and experiment. A first implementation of this idea was carried out by Clemenger[14,15] and Saunders[16] [the Clemenger-Nilsson (CN) model], who applied to metal clusters the anisotropic, harmonic-oscillator model introduced by Nilsson[10] in nuclear physics. Unfortunately, this model does not provide a full expression for the total energy of an interacting system, and therefore cannot describe either binding energies for neutral clusters or charging energies for ionic ones. Nevertheless, in spite of such shortcomings, the CN model is still widely used to interpret the data.[3,17] Naturally, such an interpretation is restricted to a handful of experimentally observable ground-state properties, i.e., abundances, IP's, and electron affinities (EA's). Moreover, for IP's and EA's the analysis is carried out at a qualitative level by following the relative shifts of the

0163-1829/95/51(3)/1902(16)/$06.00

highest-occupied-molecular-orbital (HOMO) or lowest-unoccupied-molecular-orbital (LUMO) levels.

Several Kohn-Sham local-density-approximation (KS-LDA) studies with spheroidal jellium backgrounds[18,19] have also been reported. Such KS calculations are rather time consuming and have been carried out only for a small number of sodium[18,19] and copper clusters[19] comprising less than 40 atoms and have addressed only a limited number of ground-state properties [IP's and monomer separation energies (MSE's) for Na_N, and electron affinities (EA's) for Cu_N]. Systematic theoretical results for triaxial shapes are not yet available[20] even though there exists a wealth of experimental observations for IP's, EA's, fission dissociation energies (FDE's), as well as MSE's and dimer separation energies (DSE's), which all exhibit characteristic shell effects.

In addition to the steps at shell and subshell closures, the experimental IP's, EA's, FDE's, and MSE's exhibit a characteristic odd-even alternation, which has attracted substantial interest.[21–23] One mechanism, which has been proposed[22,23] as an explanation, involves phenomenological Cooper pairing of electrons in analogy with the nuclear case, where nucleons form a BCS-type ground state.[11–13] However, it is difficult to justify[23] such a pairing in the case of clusters. Alternatively, for the IP's of simple-metal clusters, M_N, with $N \leq 9$, such odd-even alternation has been obtained in both spheroidal-jellium calculations[18] and *ab initio* quantum chemical calculations,[24] suggesting that these oscillations are of a geometric (i.e., cluster-shape) origin.

The aforementioned considerations motivate investigations aiming at a systematic assessment of relationships between observed patterns and the size evolution and dimensionality (i.e., the character and number of multipolar components) of the relevant cluster deformation spaces pertaining to the ground-state properties mentioned above. While in this study, we focus on the systematics of the influence of cluster shapes on ground-state patterns, we remark that cluster deformations have also been discussed previously in the context of optical absorption via plasmon excitations.[25–29]

In this paper, we study the influence of triaxial quadrupole shapes (ellipsoids) on the ground-state properties mentioned above and provide an extensive comparison with the available experimental data. The method adopted is a semiempirical version of the shell-correction method (SE-SCM), familiar from nuclear physics as the Strutinsky method.[30] [For other studies applying the semiempirical Strutinsky method to calculating barriers for metal cluster fission, see Refs. 31, 32, and to axially symmetric deformations for describing the optimum shapes of large neutral sodium clusters, see Ref. 33. For a microscopic LDA version of a shell-correction method (LDA-SCM), see Refs. 34–37.]

The specific elements introduced by the present work which allowed for an adaptation of the SE-SCM to metal clusters follow.

(1) Consideration of an anisotropic three-dimensional (3D) modified harmonic-oscillator potential (triaxial Nilsson potential[38]) for calculating the single-particle spectra. This potential has two advantages: (i) it allows for an easy treatment of triaxial deformations, and (ii) it allows for an analytic formula for the smooth part of the single-particle spectrum.

(2) Generalization of the liquid-drop model (which was previously considered for the ground states of neutral clusters[39,33]) to the case of the ground states of multiply cationic or anionic species (this extension is based on our previous LDA-SCM study of multiply charged clusters, modeled as spherical jellia[34,35]).

Preliminary results of our SE-SCM from triaxial droplets were presented in Refs. 34 and 35, in the context of an investigation of multiply charged anionic metal clusters.

II. SEMIEMPIRICAL SHELL-CORRECTION METHOD (STRUTINSKY METHOD)

A. Liquid-drop model for charged clusters

For neutral clusters, the liquid-drop model[40,31,39] (LDM) expresses the *smooth* part, $\widetilde{E}$, of the total energy as the sum of three contributions, namely, a volume, a surface, and a curvature term, i.e.,

$$\begin{aligned}\widetilde{E} &= E_{\rm vol} + E_{\rm surf} + E_{\rm curv} \\ &= A_v \int d\tau + \sigma \int dS + A_c \int dS\kappa \ , \end{aligned} \tag{1}$$

where $d\tau$ is the volume element and dS is the surface differential element. The local curvature κ is defined by the expression $\kappa = 0.5(R_{\rm max}^{-1} + R_{\rm min}^{-1})$, where $R_{\rm max}$ and $R_{\rm min}$ are the two principal radii of curvature at a local point on the surface of the jellium droplet which models the cluster. The corresponding coefficients can be determined by fitting the extended Thomas-Fermi- (ETF)- LDA total energy for spherical shapes[34,35,39,41] to the following parametrized expression as a function of the number N of atoms in the cluster:[42,43]

$$E_{\rm ETF}^{\rm sph} = \alpha_v N + \alpha_s N^{2/3} + \alpha_c N^{1/3} \ . \tag{2}$$

The following expressions relate the coefficients A_v, σ, and A_c to the corresponding coefficients (α's) in Eq. (2),

$$A_v = \frac{3}{4\pi r_s^3}\alpha_v \ , \ \sigma = \frac{1}{4\pi r_s^2}\alpha_s \ , \ A_c = \frac{1}{4\pi r_s}\alpha_c \ . \tag{3}$$

In the case of ellipsoidal shapes the areal integral and the integrated curvature can be expressed in closed analytical form with the help of the incomplete elliptic integrals $\mathcal{F}(\psi,k)$ and $\mathcal{E}(\psi,k)$ of the first and second kind,[44] respectively. Before writing the formulas, we need to introduce some notations. Volume conservation must be employed, namely,

$$a'b'c'/R_0^3 = abc = 1 \ , \tag{4}$$

where R_0 is the radius of a sphere with the same volume ($R_0 = r_s N^{1/3}$ is taken to be the radius of the positive jellium assuming spherical symmetry), and $a = a'/R_0$

etc., are the dimensionless semiaxes. The eccentricities are defined through the dimensionless semiaxes as

$$\begin{aligned} e_1^2 &= 1-(c/a)^2, \\ e_2^2 &= 1-(b/a)^2, \\ e_3^2 &= 1-(c/b)^2 . \end{aligned} \tag{5}$$

The semiaxes are chosen so that

$$a \geq b \geq c . \tag{6}$$

With the notation $\sin\psi = e_1$, $k_2 = e_2/e_1$, and $k_3 = e_3/e_1$, the relative (with respect to the spherical shape) surface and curvature energies are given[45] by

$$\frac{E_{\rm surf}^{\rm ell}}{E_{\rm surf}^{\rm sph}} = \frac{ab}{2}\left[\frac{1-e_1^2}{e_1}\mathcal{F}(\psi,k_3)+e_1\mathcal{E}(\psi,k_3)+c^3\right] \tag{7}$$

and

$$\frac{E_{\rm curv}^{\rm ell}}{E_{\rm curv}^{\rm sph}} = \frac{bc}{2a}\left[1+\frac{a^3}{e_1}[(1-e_1^2)\mathcal{F}(\psi,k_2)+e_1^2\mathcal{E}(\psi,k_2)]\right] . \tag{8}$$

The LDM for neutral clusters has a direct analogy with the liquid-drop model of atomic nuclei, but for charged clusters differences arise compared to the nuclear case. These differences originate from the fact that (i) the excess charge in metal clusters is distributed over the surface (classical conductor model[40,37]) instead of throughout the volume as is the case of nuclei, and (ii) the electron gas in metal clusters is treated quantum mechanically, while the positive charge of the nucleus is usually treated using classical electrostatics. As a result, in addition to an electrostatic term, the LDM for charged metal clusters has a term accounting for the size-dependent electron affinity, or ionization potential, and through it for the work function W of the bulk metal (it is to be noted that for fission processes, the information about the work function can be ignored, since its contribution cancels when considering energy differences between parent and daughter clusters).

A proper form of the LDM for charged clusters with spherical symmetry was developed by the present authors,[34,35,37] who found that the energy contribution due to the excess charge, Z, is given by

$$\Delta\widetilde{E}(Z) = \widetilde{E}(Z)-\widetilde{E}(0) = -\widetilde{A}_1 Z + \frac{Z(Z-1)e^2}{2(R_0+\delta)} \tag{9}$$

for *negatively* charged states, and by

$$\Delta\widetilde{E}(Z) = \widetilde{E}(Z)-\widetilde{E}(0) = \widetilde{I}_1 Z + \frac{Z(Z-1)e^2}{2(R_0+\delta)} \tag{10}$$

for *positively* charged states. The dependence on the number N of atoms in the cluster is not explicitly indicated. The electronic spillout-type parameter $\delta = \delta_0 + \delta_2/R_0^2$ is determined by fitting the corresponding ETF-LDA total energies (for details, see Refs. 34, 35, and 37). The smooth first electron affinity $\widetilde{A}_1$ and ionization potential $\widetilde{I}_1$ are also size dependent, and relate as follows to the bulk work function W:

$$\widetilde{A}_1 = W - \frac{5}{8}\frac{e^2}{R_0+\delta} , \quad \widetilde{I}_1 = W + \frac{3}{8}\frac{e^2}{R_0+\delta} . \tag{11}$$

Combining Eqs. (9)–(11), one gets

$$\Delta\widetilde{E}(Z) = \widetilde{E}(Z)-\widetilde{E}(0) = \mp WZ + \frac{Z(Z\pm 0.25)e^2}{2(R_0+\delta)}, \tag{12}$$

where the upper and lower signs correspond to negatively and positively charged states, respectively.

To generalize the above results to an ellipsoidal shape, $\phi(R_0+\delta) = e^2/(R_0+\delta)$, which is the value of the potential on the surface of a spherical conductor, needs to be replaced by the corresponding expression for the potential on the surface of a conducting ellipsoid. According to Ref. 46, this latter potential is given by $\frac{1}{2}e^2\int_0^\infty du/\sqrt{(u+a'^2)(u+b'^2)(u+c'^2)}$ (which is an incomplete elliptic integral of the first kind, see Eq. 3.131 of Ref. 44), and thus the final result, normalized to the spherical shape, is given by the expression

$$\frac{\Delta\widetilde{E}^{\rm ell}(Z)\pm WZ}{\Delta\widetilde{E}^{\rm sph}(Z)\pm WZ} = \frac{bc}{e_1}\mathcal{F}(\psi,k_2) , \tag{13}$$

where the $\pm$ sign in front of WZ corresponds to negatively and positively charged clusters, respectively.

B. The modified Nilsson potential

A natural choice for an external potential to be used for calculating shell corrections with the Strutinsky method is an anisotropic, three-dimensional oscillator with an $\boldsymbol{l}^2$ term for lifting the harmonic-oscillator degeneracies.[10] Such an oscillator model for approximating the total energies of metal clusters, but without separating them into a smooth and a shell-correction part in the spirit of Strutinsky's approach, has been used[3] with some success for calculating relative energy surfaces and deformation shapes of metal clusters. However, this simple harmonic-oscillator model has serious limitations, since (i) the total energies are calculated by the expression[47] $\frac{3}{4}\sum_i \varepsilon_i$, and thus do not compare with the total energies obtained from the KS-LDA approach, and (ii) the model cannot be extended to the case of charged (cationic or anionic) clusters. Thus absolute ionization potentials, electron affinities, and fission energetics cannot be calculated in this model. Alternatively, in our approach, we are making only a limited use of the external oscillator potential in calculating a modified Strutinsky shell correction. Total energies are evaluated by adding this shell correction to the smooth LDM energies.

In particular, a modified Nilsson Hamiltonian appropriate for metal clusters[14,16] is given by

$$H_N = H_0 + U_0\hbar\omega_0(\boldsymbol{l}^2 - \langle\boldsymbol{l}^2\rangle_n) , \tag{14}$$

where H_0 is the Hamiltonian for a three-dimensional anisotropic oscillator, namely,

$$H_0 = -\frac{\hbar^2}{2m_e}\Delta + \frac{m_e}{2}(\omega_1^2 x^2 + \omega_2^2 y^2 + \omega_3^2 z^2)$$
$$= \sum_{k=1}^{3}\left(a_k^\dagger a_k + \frac{1}{2}\right)\hbar\omega_k \ . \quad (15)$$

U_0 in Eq. (15) is a dimensionless parameter, which for occupied states may depend on the principal quantum number $n = n_1 + n_2 + n_3$ of the spherical-oscillator major shell associated with a given level (n_1, n_2, n_3) of the Hamiltonian H_0 (for clusters comprising up to 100 valence electrons, only a weak dependence on n is found, see Table I). U_0 vanishes for values of n higher than the corresponding value of the last partially (or fully) filled major shell in the spherical limit.

$\boldsymbol{l}^2 = \sum_{k=1}^{3} l_k^2$ is a "stretched" angular momentum which scales to the ellipsoidal shape and is defined as

$$l_3^2 \equiv (q_1 p_2 - q_2 p_1)^2 \quad (16)$$

(with similarly obtained expressions for l_1^2 and l_2^2 via a cyclic permutation of indices), where the stretched position and momentum coordinates are defined via the corresponding natural coordinates $q_k^{\rm nat}$ and $p_k^{\rm nat}$ as

$$q_k \equiv q_k^{\rm nat}(m_e\omega_k/\hbar)^{1/2} = \frac{a_k^\dagger + a_k}{\sqrt{2}} \ (k = 1,2,3) \ , \quad (17)$$

$$p_k \equiv p_k^{\rm nat}(1/\hbar m_e\omega_k)^{1/2} = i\frac{a_k^\dagger - a_k}{\sqrt{2}} \ (k = 1,2,3) \ . \quad (18)$$

The stretched $\boldsymbol{l}^2$ is not a properly defined angular-momentum operator, but has the advantageous property that it does not mix deformed states which correspond to spherical major shells with different principal quantum number $n = n_1 + n_2 + n_3$ (see the Appendix for the expression of the matrix elements of $\boldsymbol{l}^2$).

The subtraction of the term $\langle \boldsymbol{l}^2 \rangle_n = n(n+3)/2$, where $\langle\ \rangle_n$ denotes the expectation value taken over the nth-major shell in spherical symmetry, guarantees that the average separation between major oscillator shells is not affected as a result of the lifting of the degeneracy.

The oscillator frequencies can be related to the principal semiaxes a', b', and c' [see Eq. (4)] via the volume-conservation constraint and the requirement that the surface of the cluster is an equipotential one, namely,

$$\omega_1 a' = \omega_2 b' = \omega_3 c' = \omega_0 R_0 \ , \quad (19)$$

where the frequency ω_0 for the spherical shape (with radius R_0) was taken according to Ref. 15 to be

$$\hbar\omega_0(N) = \frac{49 \text{ eV bohr}^2}{r_s^2 N^{1/3}}\left[1 + \frac{t}{r_s N^{1/3}}\right]^{-2} \ . \quad (20)$$

Since in this paper we consider solely monovalent elements, N in Eq. (20) is the number of atoms for the family of clusters $M_N{}^{Z\pm}$, r_s is the Wigner-Seitz radius expressed in atomic units, and t denotes the electronic spillout for the neutral cluster according to Ref. 15.

C. Shell correction and averaging of single-particle spectra

The single-particle energies ε_i of the Hamiltonian (14) are used to obtain the semi-empirical Strutinsky shell correction, $\Delta E_{\rm sh}^{\rm Str}$, which is defined as

$$\Delta E_{\rm sh}^{\rm Str} = \sum_i^{\rm occ} \varepsilon_i - \widetilde{E}_{\rm sp} \ , \quad (21)$$

where

$$\widetilde{E}_{\rm sp} = \sum_i \varepsilon_i \widetilde{f}_i \quad (22)$$

is the Strutinsky average of the single-particle spectrum with $\widetilde{f}_i$ being appropriate weighting factors.

Usually $\widetilde{E}_{\rm sp}$ is calculated numerically.[48] However, a variation of the numerical Strutinsky averaging method

TABLE I. Parameters entering into the SE-SCM calculations. U_0 is a dimensionless parameter [see Eq. (14)]. All lengths, i.e., for the Wigner-Seitz radius r_s, and the spillout parameters t [see Eq. (20)] and δ_0 (see Sec. II A) are expressed in a.u. δ_2 (see Sec. II A) is expressed in (a.u.)^3. Energies for the bulk work function W [see Eq. (11)], and for the coefficients α_v, α_s, and α_c [see Eq. (3)] are in eV.

	U_0	r_s	$t^{\rm a}$	δ_0	δ_2	$W^{\rm a}$	α_v	α_s	α_c
Na	0.040 ($n = 2-4$)	4.00	1.44	1.16 ($z=-1$)$^{\rm b}$	23.33 ($z=-1$)$^{\rm b}$	2.70	$-2.252^{\rm b}$	$0.541^{\rm b}$	$0.154^{\rm b}$
	0.035 ($n \geq 5$)			0.00 ($z=+1$)$^{\rm b}$	0.00 ($z=+1$)$^{\rm b}$				
K	0.040 ($n = 2-4$)	4.86	1.78	1.51 ($z=-1$)$^{\rm b}$	0.00 ($z=-1$)$^{\rm b}$	2.39	$-2.198^{\rm b}$	$0.521^{\rm b}$	$0.072^{\rm b}$
	0.035 ($n \geq 5$)			0.00 ($z=+1$)$^{\rm b}$	0.00 ($z=+1$)$^{\rm b}$				
Cu	0.030	2.67	0.78	1.28 ($z=-1$)$^{\rm c}$	0.00 ($z=-1$)$^{\rm c}$	4.65	$-8.875^{\rm c}$	$0.721^{\rm c}$	$0.359^{\rm c}$
				0.00 ($z=+1$)$^{\rm c}$	0.00 ($z=+1$)$^{\rm c}$				

[a]Experimental values according to a compilation of Ref. 15.

[b]Specified through a fit of Eq. (2) to ETF-LDA total energy calculations for spherical clusters in conjunction with the jellium-background approximation [see Refs. 34 and 35].

[c]Specified through a fit of Eq. (2) to ETF total energy calculations for spherical clusters in conjunction with a *stabilized-jellium*-LDA energy functional [see Ref. 37].

consists in using the semiclassical partition function and in expanding it in powers of $\hbar^2$. With this method, for the case of an anisotropic, fully triaxial oscillator, one finds[11,49] an analytical result, namely,[50]

$$\widetilde{E}_{\rm sp}^{\rm osc} = \hbar(\omega_1\omega_2\omega_3)^{1/3} \times \left(\frac{1}{4}(3N_e)^{4/3} + \frac{1}{24}\frac{\omega_1^2+\omega_2^2+\omega_3^2}{(\omega_1\omega_2\omega_3)^{2/3}}(3N_e)^{2/3}\right) , \quad (23)$$

where N_e denotes the number of delocalized valence electrons in the cluster.

In the present work, expression (23) (as modified below) will be substituted for the average part $\widetilde{E}_{\rm sp}$ in Eq. (21), while the sum $\sum_i^{\rm occ}\varepsilon_i$ will be calculated numerically by specifying the occupied single-particle states of the modified Nilsson oscillator represented by the Hamiltonian (14).

In the case of an isotropic oscillator, not only the smooth contribution $\widetilde{E}_{\rm sp}^{\rm osc}$ but also the Strutinsky shell correction (21) can be specified analytically,[11] with the result

$$\Delta E_{\rm sh,0}^{\rm Str}(x) = \frac{1}{24}\hbar\omega_0(3N_e)^{2/3}[-1+12x(1-x)] , \quad (24)$$

where x is the fractional filling of the highest partially filled harmonic-oscillator shell. We see that for a filled shell ($x=0$), $\Delta E_{\rm sh,0}^{\rm Str}(0) = -\frac{1}{24}\hbar\omega_0(3N_e)^{2/3}$, instead of the essentially vanishing value as in the case of the ETF-LDA defined shell correction (cf. Fig. 1). To adjust for this discrepancy, we add $-\Delta E_{\rm sh,0}^{\rm Str}(0)$ to $\Delta E_{\rm sh}^{\rm Str}$ calculated through Eq. (21) for the case of open-shell, as well as closed-shell clusters.

D. Overall procedure

We are now in a position to summarize the calculational procedure, which consists of the following steps.

(1) Parametrize results of ETF-LDA calculations for spherical neutral jellia according to Eq. (2).

(2) Use above parametrization (assuming that parameters per differential element of volume, surface, and integrated curvature are shape independent) in Eq. (1) to calculate the liquid-drop energy associated with neutral clusters, and then add to it the charging energy according to Eq. (13) to determine the total LDM energy $\widetilde{E}$.

(3) Use Eqs. (14) and (15) for a given deformation [i.e., a', b', c', or equivalently ω_1, ω_2, ω_3, see Eq. (19)] to solve for the single-particle spectrum (ε_i).

(4) Evaluate the average, $\widetilde{E}_{\rm sp}$, of the single-particle spectrum according to Eq. (23) and subsequent remarks.

(5) Use the results of steps (3) and (4) above to calculate the shell correction $\Delta E_{\rm sh}^{\rm Str}$ according to Eq. (21).

(6) Finally, calculate the total energy $E_{\rm sh}$ as the sum of the liquid-drop contribution [step (2)] and the shell correction [step (5)], namely, $E_{\rm sh} = \widetilde{E} + \Delta E_{\rm sh}^{\rm Str}$.

The optimal ellipsoidal geometries for a given cluster $M_N{}^{Z\pm}$, neutral or charged, are determined by systematically varying the distortion (namely, the parameters a and b) in order to locate the global minimum of the total energy $E_{\rm sh}(N,Z)$.

To illustrate the quantitative quality of results obtained by our present method, we exhibit in Fig. 2 per atom total energies (normalized to the bulk value $|\varepsilon_\infty| = 2.252$ eV) calculated by us for Na_N clusters. In Fig. 2(a), results obtained for spherical symmetry are contrasted with corresponding results for spheroidally deformed clusters. The effect of triaxial deformations is demonstrated in Fig. 2(b). While a detailed discussion of the consequences of various deformation models will be presented in Sec. III, we remark here on the quantitative agreement between the results of Fig. 2 and correspond-

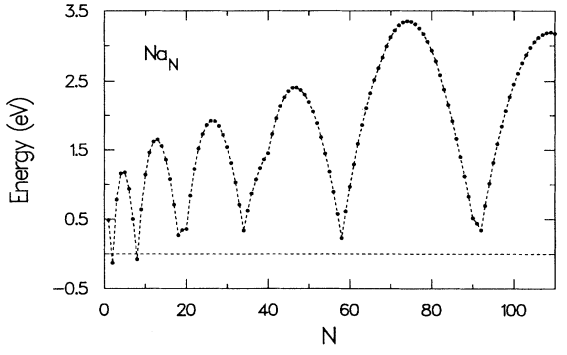

FIG. 1. The LDA-SCM shell correction for spherical neutral sodium clusters in the range $1 \le N \le 100$.

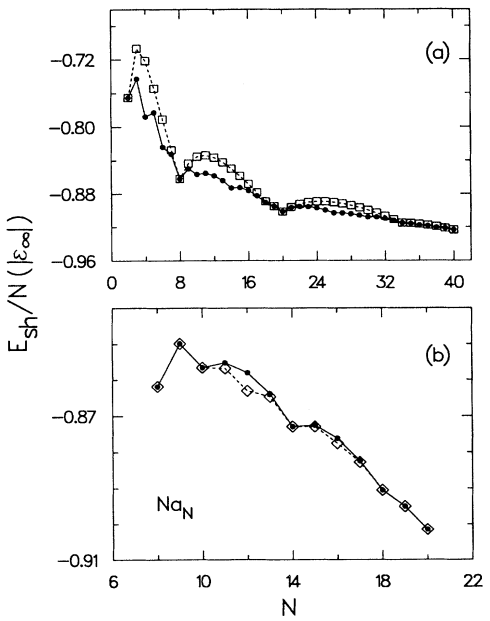

FIG. 2. SE-SCM results for the total energy per atom of neutral sodium clusters Na_N (in units of the absolute value of the energy per atom in the bulk, $|\varepsilon_\infty| = 2.252$ eV). (a) Open squares: results for spherical symmetry. Solid dots: results for the spheroidal model. (b) Solid dots: results for the spheroidal model. Open diamonds: results for the ellipsoidal model.

ing results obtained via self-consistent KS-LDA calculations [i.e., for spherical and spheroidal sodium clusters, compare Fig. 2(a) with Fig. 1 of Ref. 18 and for spheroidal and triaxial deformations compare Fig. 2(b) with Fig. 3 of Ref. 51 (note that in Ref. 51 the triaxial calculations for neutral sodium clusters were performed only for clusters with an even number of atoms in the range $8 \leq N \leq 20$, and consequently odd-even alternations in the total energy were not seen)].

III. RESULTS

The different parameters used in the present SE-SCM calculations are summarized in Table I.

A. Ionization potentials

We have calculated ionization potentials by subtracting two ground-state energies, namely, the ground-state energy of the neutral clusters from the ground-state energy of the singly charged cations,

$$I_{\rm sh}(N) = E_{\rm sh}(z = +1, N) - E_{\rm sh}(z = 0, N) \ . \qquad (25)$$

Note that the lower case z in Eq. (25) denotes the algebraic value of the excess charge, namely, $z < 0$ for anions, $z > 0$ for cations, and $|z| = Z$.

1. Potassium clusters

The theoretical results compared to the experimental measurements[16,52] for the case of potassium clusters, K_N, are displayed in Fig. 3 in the range $2 \leq N \leq 100$. The inset of the figure displays the theoretical results in the case of spherical shapes compared to the experimental measurements. The theoretical results in the latter case exhibit a pronounced sawtoothed profile which, with the exception of major-shell closures, is in poor agreement with the experiment, a trend previously known from LDA calculations on spherical jellia.[5,2,35]

Consideration of triaxial deformations leads to a substantial improved correspondence between the theoretical and experimental results, especially pertaining to the following two trends: (i) between major-shell closures, the overall shape of the theoretical curve is flat, resembling staircases as is exhibited by the data, and (ii) noticeable fine structure has replaced the monotonous sawtooths of the spherical case.

An inspection of the theoretical curve reveals that the fine structure exhibits a pronounced odd-even oscillation for sizes up to $N = 21$ electrons. A comparable odd-even oscillation is also seen in the experimental data. For sizes larger than 20 electrons, the odd-even oscillations are not present in the experimental data (unlike the case of low-temperature sodium clusters to be discussed below), presumably because of the high internal temperatures of the clusters in this experiment. Nevertheless, the data do show the expected major-shell closures, and in addition they exhibit signatures of subshell closures at $N = 26$ and $N = 30$ electrons. Overall, these trends are reproduced by the theoretical results (in particular, the $N = 26$ and $N = 30$ subshell closures are clearly evident). We note that for $N > 21$ electrons the importance of nonaxial shapes decreases noticeably, and as a result the theoretical odd-even effect weakens to the extent that the theoretical points exhibit several well-defined quartets (i.e., for $N = 21 - 24$, $N = 27 - 30$, or $N = 31 - 34$), which are a reflection of four-fold degeneracies compati-

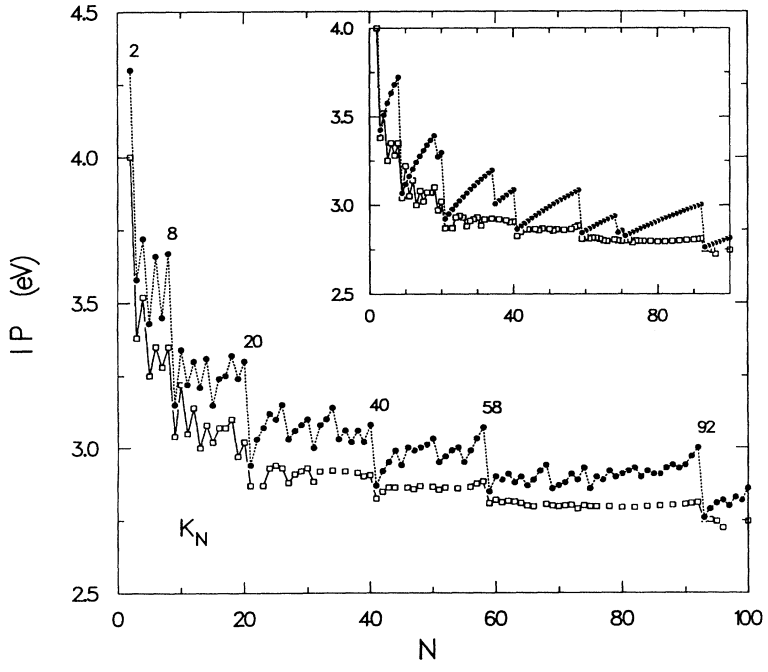

FIG. 3. IP's for K_N clusters in the range $2 \leq N \leq 100$. Solid dots: Theoretical results derived from the SE-SCM method in conjuction with the ellipsoidal model. Open squares: Experimental measurements from Ref. 16. The inset displays corresponding IP's derived from the SE-SCM (solid dots) in conjunction with the spherical model.

ble with axial symmetry.

We stress that the agreement between theory and experiment in the range $N = 2 - 21$ is particularly good and detailed. Indeed, not only is the overall odd-even oscillatory pattern predicted by the theory, but even a subtler feature, namely, the absence of a sharp odd-even step in the quartet $N = 15 - 18$, is well reproduced.

We conclude that, for potassium clusters, the triaxial Strutinsky method yields an excellent detailed agreement between theory and experiment for sizes smaller than 21 electrons. For larger sizes, theory still provides a good agreement, in spite of the diminishing weight of triaxiality, but this agreement is expected to degrade at lower temperatures due to an anticipated reappearance of odd-even alternations in the size range above 21 electrons (see discussions on IP's for cold copper and sodium clusters below).

2. *Copper clusters*

Ionization potentials of cold copper clusters have recently been measured.[53] These results are displayed in Fig. 4 together with our theoretical results for Cu_N clusters with $3 \leq N \leq 43$.

To illustrate and elucidate the influence of cluster shapes on the IP's, we have carried out calculations for all three shape families, namely, spherical, spheroidal, and ellipsoidal deformations. An inspection of Fig. 4 reveals that spherical shapes (top panel) exhibit the characteristic sawtoothed profile, and that, apart from major-shell closures, they describe the data rather poorly (note in particular the absence of fine structure and the presence of an exaggerated amplitude in the sawtoothed modulation).

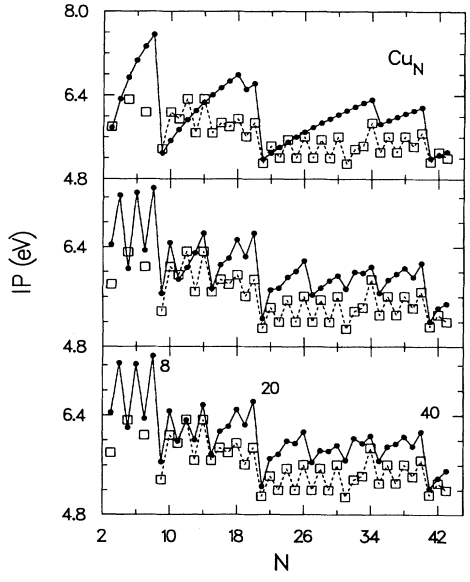

FIG. 4. IP's for Cu_N clusters in the range $3 \leq N \leq 43$. Solid dots: Theoretical results derived from the SE-SCM method. Open squares: Experimental measurements from Ref. 53. Experimental data for $N = 4$, 6, and 8 are not available. Top panel: The spherical model compared to experimental data. Middle panel: The spheroidal model compared to experimental data. Lower panel: The ellipsoidal model compared to experimental data.

The spheroidal model (middle panel) shows substantial improvement in coming closer to the experimental trend. Furthermore, the ellipsoidal case (bottom panel) improves the agreement between theory and experiment even further. A noticeable improvement concerns the better description of odd-even alternations between the steps at shell and subshell closures (the subshell closures appear at $N = 14$, 26, and 30). Again, as was the case with potassium, the spheroidal quartet $N = 11 - 14$ is strongly perturbed and exhibits strong odd-even alternations in accordance with the data. On the contrary, the quartet $N = 15 - 18$ remains almost unaltered in agreement with the observation. The amplitude of the theoretical odd-even alternations above $N = 21$ is smaller than the experimentally observed one, however, the overall trend is reproduced. We note that the experiment exhibits a well-defined quartet at $N = 31 - 34$, which is also evident in the theoretical results.

3. *Sodium clusters*

Most recently, systematic measurements of the IP's of cold sodium clusters, Na_N, were performed.[54] The SE-SCM results (for N up to 105 atoms) as well as the experimental data are displayed in Fig. 5. The overall agreement between theory and experiment is very satisfactory (note the close quantitative agreement of the absolute IP values). The steps at major-shell closings ($N = 8$, 20, 40, 58, 92), as well as those at subshell closings ($N = 14$, 26, 30, 34, 44, 50, 54, 68), are comparable to the experimental ones. Additionally the theoretical results reproduce

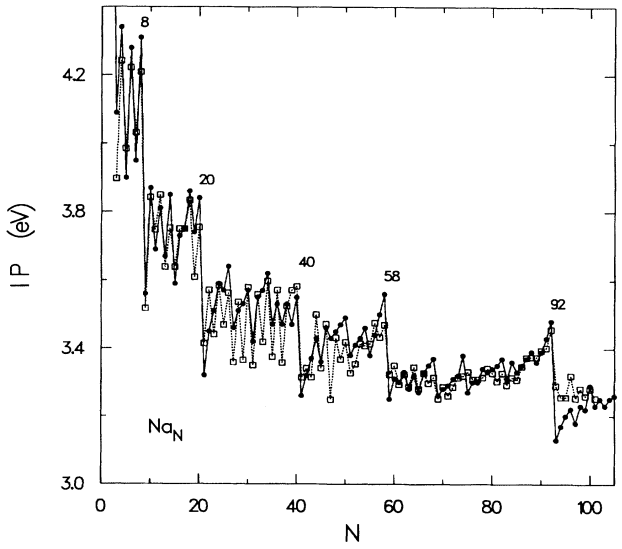

FIG. 5. IP's for Na_N clusters in the range $3 \leq N \leq 105$. Solid dots: Theoretical results derived from the SE-SCM method in conjunction with the ellipsoidal model. Open squares: Experimental measurements from Ref. 54.

well the staircase profile of the experimental curve. The overall weakening of the oscillations of the fine structure with increasing size seen in the experimental data is also portrayed by the calculations.

The odd-even oscillations are accurately reproduced for $3 \leq N \leq 21$. Above $N = 21$, however, the theory provides only a partial account for the odd-even alternations (i.e., for $N = 35 - 40$, $N = 59 - 65$, and $N = 95 - 101$). Here, experimentally observed odd-even oscillations are present throughout the $N = 21 - 40$ region and in the beginnings of the major shells immediately after $N = 40$ and $N = 58$.

4. *The size range $N = 3 - 21$*

As aforementioned, ellipsoidal shapes reproduce especially well the trends in the experimental IP's in the region $3 \leq N \leq 21$. To further elaborate on this agreement, we show in Fig. 6 and Fig. 7 a magnification of this size region with respect to the IP curves of potassium and sodium clusters. Theoretical results for exclusively spheroidal shapes are also displayed, in order to further demonstrate the improvement resulting from the consideration of triaxial deformations. The spheroidal model reproduces well the odd-even oscillation in the range $N = 2 - 9$, but fails in the range $N = 9 - 21$. In fact, in this latter range, two well-formed quartets ($N = 11 - 14$ and $N = 15 - 18$) are prominent in the upper panels of Fig. 6 and Fig. 7 (as well as in the middle panel of Fig. 4 for the copper case), and result from the four-fold degeneracy characteristic of the axial symmetry.[19] On the other hand, consideration of triaxial shapes lifts this degeneracy [see also Fig. 2(b), Fig. 3, Fig. 4, and Fig. 5] and allows for the strong odd-even effects for $N = 11 - 14$, while at the same time producing a very weak (practically, the odd-even alternation is absent in accordance with the experiment) modification for $N = 15 - 18$. It is apparent that triaxiality is necessary to account for all the details of the data.

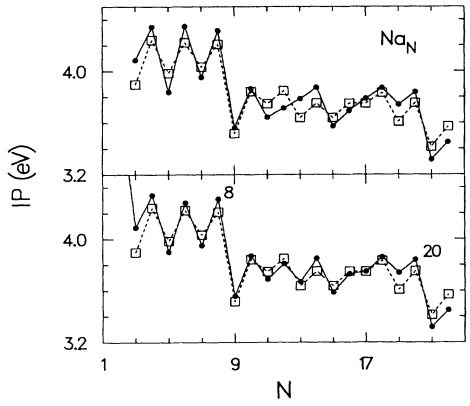

FIG. 6. IP's for Na_N clusters in the range $3 \leq N \leq 22$. Solid dots: Theoretical results derived from the SE-SCM method. Open squares: Experimental measurements from Ref. 54. Top panel: The spheroidal model compared to experimental data. Lower panel: The ellipsoidal model compared to experimental data.

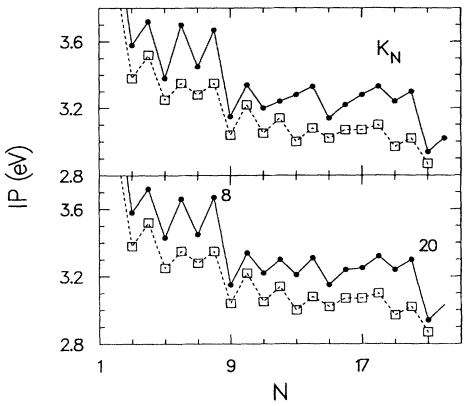

FIG. 7. IP's for K_N clusters in the range $3 \leq N \leq 22$. Solid dots: Theoretical results derived from the SE-SCM method. Open squares: Experimental measurements from Ref. 16. Top panel: The spheroidal model compared to experimental data. Lower panel: The ellipsoidal model compared to experimental data.

We note that the proposed explanation of odd-even alternations as originating from phenomenological pairing forces fails to describe this behavior, since it predicts as strong odd-even alternations for $N = 15 - 18$ as those for $N = 11 - 14$.[22,23]

We will see below that the exceptionally accurate agreement between theory and experiment in this size range is not limited to IP's, but extends to all the quantities studied, namely, electron affinities, monomer and dimer separation energies, and fission-channel energetics. In particular, the feature concerning the appearance of strong odd-even oscillations for $N = 11-14$ simultaneously with the preservation of the quartet for $N = 15-18$ is also present in the electron affinities and monomer separation energies.

B. Electron affinities

Electron affinities have been determined by us as the difference between two ground-state energies, namely, by subtracting the ground-state energy of the singly charged anions from the ground-state energy of the neutral clusters,

$$A_{\rm sh}(N) = E_{\rm sh}(z = 0, N) - E_{\rm sh}(z = -1, N) \ . \qquad (26)$$

The theoretical results for Cu_N and K_N are displayed in Fig. 8 and Fig. 9, respectively, and are compared to the experimental measurements (Ref. 55 for Cu_N and Ref. 17 for K_N). Again, in both cases, the sawtoothed profile associated with spherical jellia compares rather poorly with the experimental data. We note that the magic numbers (8, 18, 20, 34, 40) are associated with the minima of the EA curve. Noticeable improvement in the agreement between theory and experiment is achieved when spheroidal shapes are considered (middle panels). Consideration of ellipsoidal shapes (bottom panels) results in a detailed

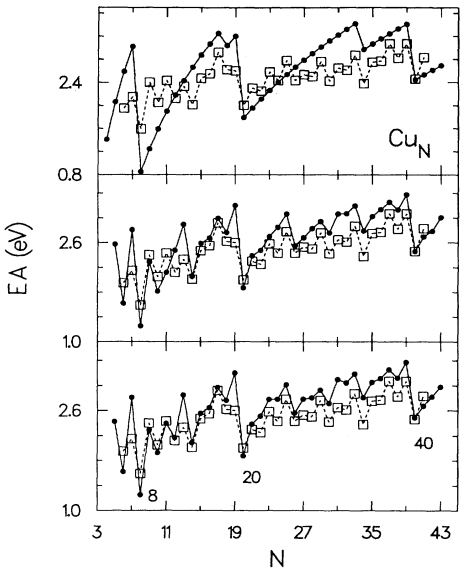

FIG. 8. EA's for Cu_N clusters in the range $5 \leq N \leq 43$. Solid dots: Theoretical results derived from the SE-SCM method. Open squares: Experimental measurements from Ref. 55. Top panel: The spherical model compared to experimental data. Middle panel: The spheroidal model compared to experimental data. Lower panel: The ellipsoidal model compared to experimental data.

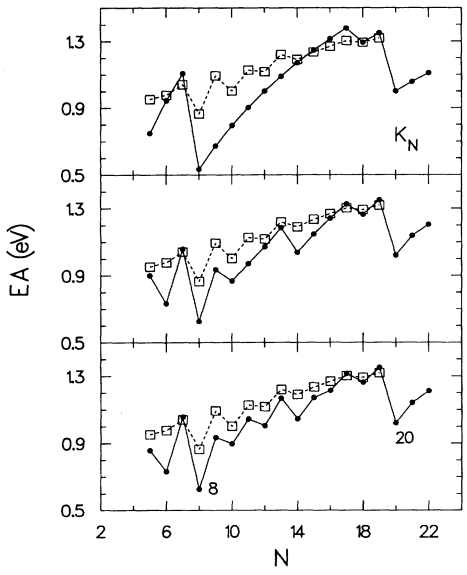

FIG. 9. EA's for K_N clusters in the range $5 \leq N \leq 22$. Solid dots: Theoretical results derived from the SE-SCM method. Open squares: Experimental measurements from Ref. 17. Top panel: The spherical model compared to experimental data. Middle panel: The spheroidal model compared to experimental data. Lower panel: The ellipsoidal model compared to experimental data.

agreement between theory and experiment, mainly due to the enhancement of odd-even oscillations. In particular, the feature of strong odd-even oscillations in the range $N = 10 - 13$ together with the preservation of the quartet structure for $N = 14 - 17$ is evident in both the Cu_N and K_N cases, and is accounted for only by the triaxial calculations. In the case of copper, the presence of another well-defined quartet at $N = 34 - 37$ is also accurately reproduced by the triaxial calculations. We also note that triaxiality offers a detailed agreement for the odd-even alternations in the EA curve of Cu_N up to $N = 41$.

C. Monomer and dimer separation energies

Monomer and dimer separation energies associated with the unimolecular reactions $K_N{}^+ \rightarrow K_{N-1}{}^+ + K$, $K_N{}^+ \rightarrow K_{N-2}{}^+ + K_2$, and $Na_N{}^+ \rightarrow Na_{N-1}{}^+ + Na$ have also been calculated as follows:

$$D_{1,N}{}^+ = E_{\rm sh}(z = +1, N-1) + E_{\rm sh}(z = 0, N = 1) - E_{\rm sh}(z = +1, N) \quad (27)$$

and

$$D_{2,N}{}^+ = E_{\rm sh}(z = +1, N-2) + E_{\rm sh}(z = 0, N = 2) - E_{\rm sh}(z = +1, N)\ . \quad (28)$$

The theoretical results for $D_{1,N}{}^+$ and $D_{2,N}{}^+$ for potassium are displayed in Fig. 10 and Fig. 11, respectively, and are compared to the experimental measurements.[56] The theoretical and experimental[57] results for $D_{1,N}{}^+$ in the case of sodium are displayed in Fig. 12. An inspection of all three figures leads to the same conclusion as for the case of IP's and EA's, i.e., that results obtained via calculations restricted to spherical shapes compare rather poorly with the experiment, that improvement is evident when spheroidal deformations are considered, and that the agreement between theory and experiment becomes detailed when triaxiality is taken into consideration. The feature of the appearance of strong odd-even alternations for $N = 12 - 15$ (note the one-unit shift due to the single positive excess charge) together with a well-defined quartet in the range $N = 16 - 19$ is present in the monomer separation energies of both potassium and sodium clusters, and is again accounted for only after the inclusion of triaxial deformations.

We note that in the case of dimer separation energies (Fig. 11) the odd-even alternations cancel out. Parents with closed shells or subshells correspond to maxima, while daughters with closed shells or subshells are associated with minima (e.g., the triplets $N = 9 - 11$, or $N = 15 - 17$).

D. Fission energetics

Fission of doubly charged metal clusters, $M_N{}^{2\pm}$, has attracted considerable attention in the last few years.

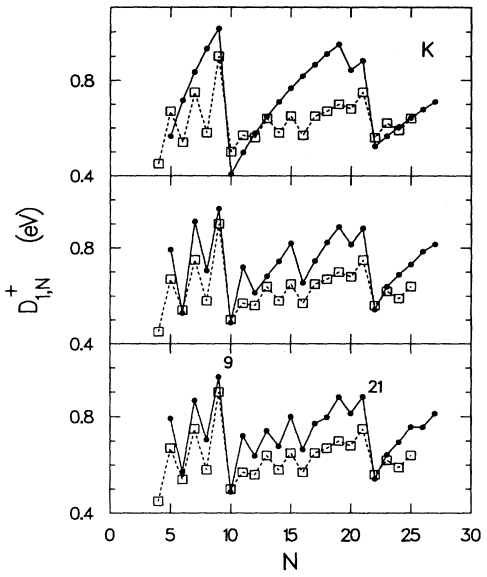

FIG. 10. Monomer separation energies, $D_{1,N}{}^+$ [see Eq. (27)], from singly cationic $K_N{}^+$ clusters in the range $5 \leq N \leq 27$. Solid dots: Theoretical results derived from the SE-SCM method. Open squares: Experimental measurements from Ref. 56. Top panel: The spherical model compared to experimental data. Middle panel: The spheroidal model compared to experimental data. Lower panel: The ellipsoidal model compared to experimental data.

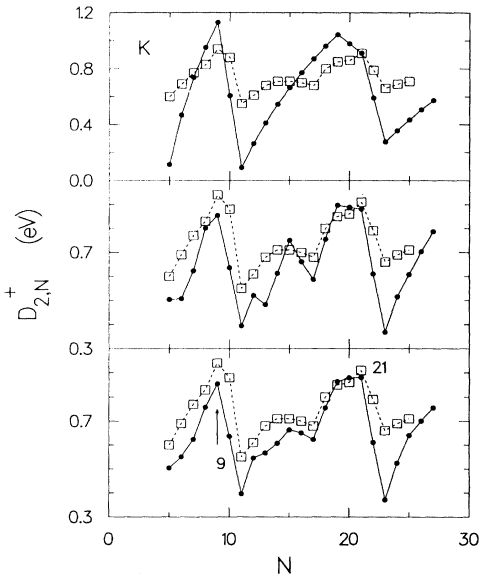

FIG. 11. Dimer separation energies, $D_{2,N}{}^+$ [see Eq. (28)], from singly cationic $K_N{}^+$ clusters in the range $5 \leq N \leq 27$. Solid dots: Theoretical results derived from the SE-SCM method. Open squares: Experimental measurements from Ref. 56. Top panel: The spherical model compared to experimental data. Middle panel: The spheroidal model compared to experimental data. Lower panel: The ellipsoidal model compared to experimental data.

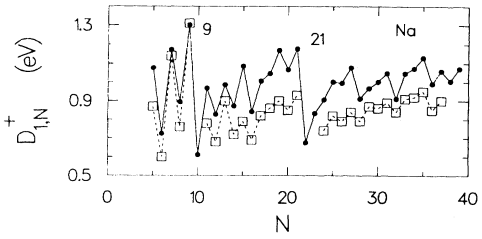

FIG. 12. Monomer separation energies, $D_{1,N}{}^+$ [see Eq. (27)], from singly cationic $Na_N{}^+$ clusters in the range $5 \leq N \leq 39$. Solid dots: Theoretical results derived from the SE-SCM method. Open squares: Experimental measurements from Ref. 57.

Nevertheless, LDA calculations have been restricted to spherical jellia for both parent and daughters,[58,59] with the exception of molecular-dynamical calculations for sodium[60] and potassium[61] clusters with $N \leq 12$. We present here systematic calculations for the dissociation energies $\Delta_{N,P}$ of the fission processes $K_N{}^{2+} \rightarrow K_P{}^+ + K_{N-P}{}^+$, as a function of the fission channels P.

We have calculated the dissociation energies

$$\Delta_{N,P} = E_{\rm sh}(z=+1,P) + E_{\rm sh}(z=+1,N-P) - E_{\rm sh}(z=+2,N)\ , \tag{29}$$

for the cases of parent clusters having $N = 26$, 23, 18, and 15 potassium atoms, for which corresponding experimental results[62] are available. The theoretical calculations compared to the experimental results are displayed in Figs. 13–16 for $N = 26$, 23, 18, 15, respectively. Again, while consideration of spheroidal shapes improves greatly the agreement between theory and experiment over the spherical model, fully detailed correspondence is achieved only upon allowing for triaxial-shape deformations (notice the improvement in the range $P = 12 - 14$ for $N = 26$, and in the range $P = 10 - 13$ for $N = 23$). In the cases $N = 18$ and $N = 15$ (Fig. 15 and Fig. 16), the biaxial and triaxial results are essentially identical, since no fragment with more than nine electrons is involved. We note that the magic fragments $K_3{}^+$ and $K_9{}^+$ correspond always to strong minima, and that for $N = 18$ the channel associated with the double magic fragments ($K_9{}^+$, $K_9{}^+$) is clearly the favored one over the other magic channel with $K_3{}^+$, in agreement with the experimental analysis. Finally, we carried out calculations of dissociation energies, $\Delta_f^{\rm pos}$ and $\Delta_f^{\rm neg}$, of the most favored fission channels over the whole range up to $N = 100$ atoms for the cases of doubly charged cationic and anionic sodium clusters, respectively. The triaxial results compared to the spherical-jellia calculations according to the LDA-SCM method[35] are displayed[63] in Fig. 17 and Fig. 18. In both cases, the main difference from the spherical jellium is a strong suppression of the local minima, indicating that the critical size for exothermic fission is significantly smaller than $N = 100$, as indeed has been observed experimentally for hot cationic alkali-metal clusters.[62]

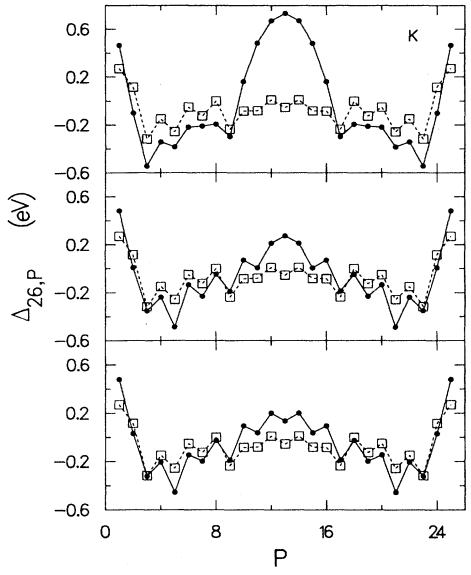

FIG. 13. Fission dissociation energies, $\Delta_{26,P}$ [see Eq. (29)], for the doubly cationic K_{26}^{2+} cluster as a function of the fission channels P. Solid dots: Theoretical results derived from the SE-SCM method. Open squares: Experimental measurements from Ref. 62. Top panel: The spherical model compared to experimental data. Middle panel: The spheroidal model compared to experimental data. Lower panel: The ellipsoidal model compared to experimental data.

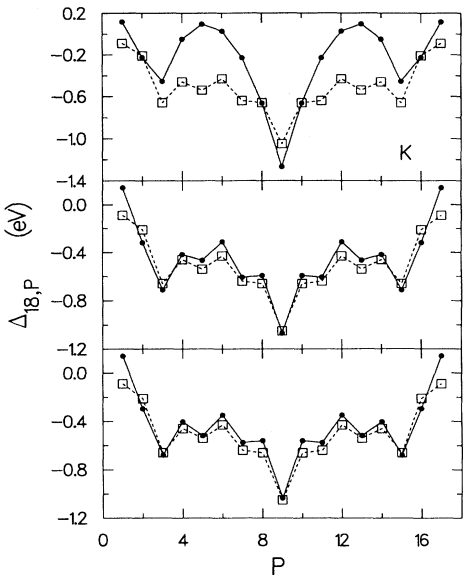

FIG. 15. Fission dissociation energies, $\Delta_{18,P}$ [see Eq. (29)], for the doubly cationic K_{18}^{2+} cluster as a function of the fission channels P. Solid dots: Theoretical results derived from the SE-SCM method. Open squares: Experimental measurements from Ref. 62. Top panel: The spherical model compared to experimental data. Middle panel: The spheroidal model compared to experimental data. Lower panel: The ellipsoidal model compared to experimental data.

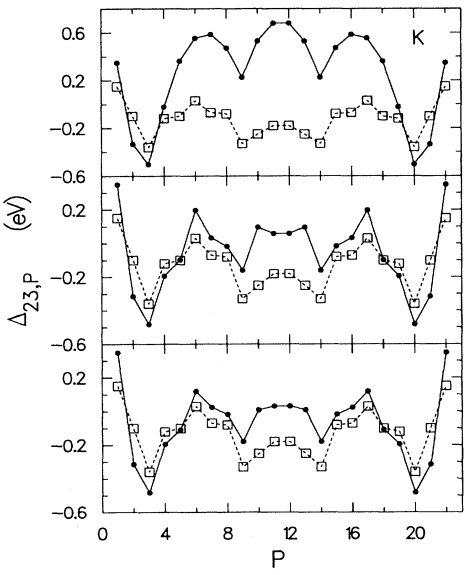

FIG. 14. Fission dissociation energies, $\Delta_{23,P}$ [see Eq. (29)], for the doubly cationic K_{23}^{2+} cluster as a function of the fission channels P. Solid dots: Theoretical results derived from the SE-SCM method. Open squares: Experimental measurements from Ref. 62. Top panel: The spherical model compared to experimental data. Middle panel: The spheroidal model compared to experimental data. Lower panel: The ellipsoidal model compared to experimental data.

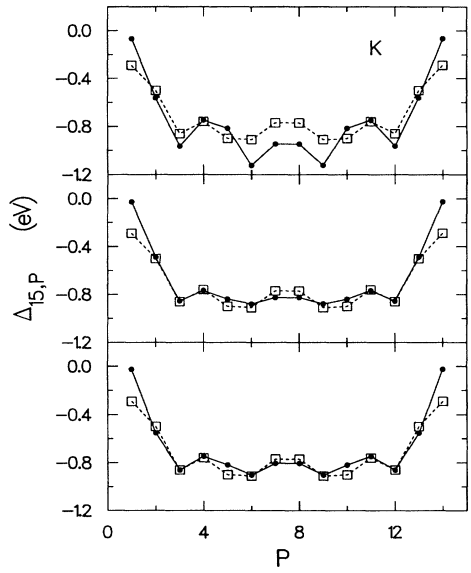

FIG. 16. Fission dissociation energies, $\Delta_{15,P}$ [see Eq. (29)], for the doubly cationic K_{15}^{2+} cluster as a function of the fission channels P. Solid dots: Theoretical results derived from the SE-SCM method. Open squares: Experimental measurements from Ref. 62. Top panel: The spherical model compared to experimental data. Middle panel: The spheroidal model compared to experimental data. Lower panel: The ellipsoidal model compared to experimental data.

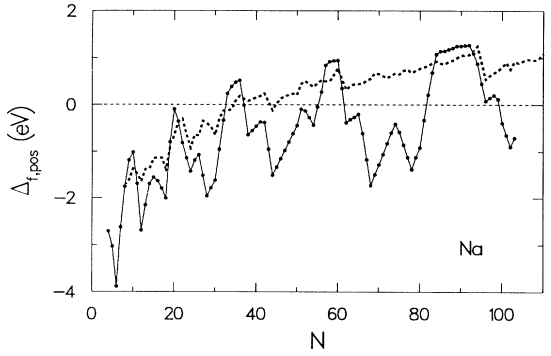

FIG. 17. Solid dots: LDA-SCM results for the dissociation energies Δ_f^{pos} for the most favorable fission channel for doubly charged cationic parents $Na_N{}^{2+}$ when the spherical jellium is used. The influence of triaxial deformation effects (calculated with the SE-SCM approach) is shown by the thick dashed line.

E. Cluster shapes

In this subsection, we present systematics of the Na_N equilibrium triaxial shapes in the range $3 \leq N \leq 60$. A most economical way for such a presentation is through the use of the Hill-Wheeler parameters[64] β and γ, which are related to the dimensionless semiaxes a, b, and c [see Eq. (4)] as follows:

$$a = \exp\left[\sqrt{5/(4\pi)}\,\beta\cos\left(\gamma - \frac{2\pi}{3}\right)\right],$$
$$b = \exp\left[\sqrt{5/(4\pi)}\,\beta\cos\left(\gamma + \frac{2\pi}{3}\right)\right], \qquad (30)$$
$$c = \exp\left[\sqrt{5/(4\pi)}\,\beta\cos\gamma\right],$$

where β is unrestricted and $0 \leq \gamma \leq \pi/3$. A value $\gamma \neq 0$ indicates a triaxial shape, while $\gamma = 0$ corresponds to a prolate shape, and $\gamma = \pi/3$ denotes an oblate deformation. The origin corresponds to spherical shapes.

Using the above definitions, the cluster potential energy surfaces (PES's) in deformation space may be easily mapped and studied (see Sec. II D). In this manner, one can analyze the topography of the PES's, identify global as well as local minima (i.e., shape isomers), barriers separating them, and paths in deformation space by which they may transform to each other. Since the values of ground-state properties of clusters depend on the shape of the cluster, the existence of shape isomers may be manifested in experimental measurements. For example, in the case of measurements of ionization potentials, vertical ionization of a cluster M_N (e.g., starting from its optimal ground-state configuration, or close to it) results in an $M_N{}^+$ cluster in the configuration of the parent neutral. If the $M_N{}^+$ cluster possesses shape isomers, it may relax either to the optimal configuration (global minimum) or to a local minimum (shape isomer), depending on the relationship between the topology of the PES for the $M_N{}^+$ cluster and that of the M_N parent. These two channels will lead to different values for the adiabatic IP. Moreover, the measured IP value may depend on the internal energy of the cluster (i.e., internal kinetic energy, or temperature), since the rate of shape transformations is expected to be enhanced at higher temperatures (i.e., at low temperature the cluster may be trapped at local minima in "shape space"). We suggest that measurements of cluster properties, and their temperature dependence, may provide information about the topology of the PES's of clusters in shape space. Indeed, evidence for the occurrence of structural isomers has been inferred from photoionization studies[65] of niobium clusters, where multiple ionization energies were measured for Nb_9 and Nb_{12}, and from kinetic studies[65,66] of the reactivity behavior of niobium clusters reacting with D_2.

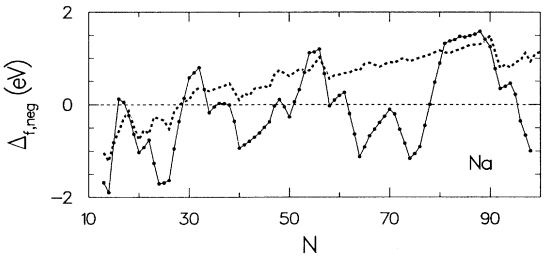

FIG. 18. Solid dots: LDA-SCM results for the dissociation energies Δ_f^{neg} for the most favorable fission channel for doubly charged anionic parents $Na_N{}^{2-}$ when the spherical jellium is used. The influence of triaxial deformation effects (calculated with the SE-SCM approach) is shown by the thick dashed line.

The PES's for Na_{12}, Na_{13}, and Na_{14} are shown in Fig. 19 using the Hill-Wheeler parametrization. First we note that all three clusters possess at least one shape isomer. For Na_{12}, the optimal shape is triaxially deformed and is separated by a potential barrier of approximately 0.5 eV from a shallow oblate isomer. On the other hand, for Na_{13}, while the optimal shape is triaxial close to the prolate axis, there exists a triaxial-shape isomer close to the oblate axis. We note that the energy difference between the two minima is very small, reflecting the fact that the topology of the PES of Na_{13} is characterized by a very flat valley in the γ coordinate. This is correlated with the insensitivity of the total energy of this cluster calculated via the spheroidal and ellipsoidal models [see Fig. 2(b)]. In this context, we remark that the above observation concerning the flat nature of the Na_{13} PES is in agreement with conclusions drawn from LDA molecular-dynamics calculations.[67] Finally, the PES for Na_{14} exhibits two axially symmetric minima, with the global one being the oblate shape.

The PES for the case of a spherical cluster is shown in Fig. 20 (upper panel) for Na_{20}. Triaxial-shape isomerization corresponding to variation of the β coordinate (distinguished from that for Na_{13} where shape isomerization involves variation of the γ deformation parameter) is illustrated in Fig. 20 (lower panel) for Na_{23}.

In Fig. 21 and Fig. 22, we present the Hill-Wheeler parameters which correspond to the global minima of the total energy of the clusters within our SE-SCM approach. Results are shown for both the spheroidal (Fig. 21) and ellipsoidal (Fig. 22) models. We note that, as a result of

allowing for ellipsoidal deformations, many clusters assume well-developed triaxial shapes, most notably Na_5, Na_{11}, Na_{12}, Na_{13}, Na_{16}, etc. Overall the extent of deformation decreases with increasing size, as reflected in the diminishing values of the β parameter. As expected, clusters associated with major-shell closures lie at the origin (i.e., they are spherical), except Na_{18}, which has an oblate shape.

Unlike the present work, where deformed shapes are inferred through ground-state properties, earlier this was usually done through photoabsorption measurements.[3,25–27] Indeed, phenomenological models assign a different absorption energy for each axis and divide the oscillator strength equally among them (1/3

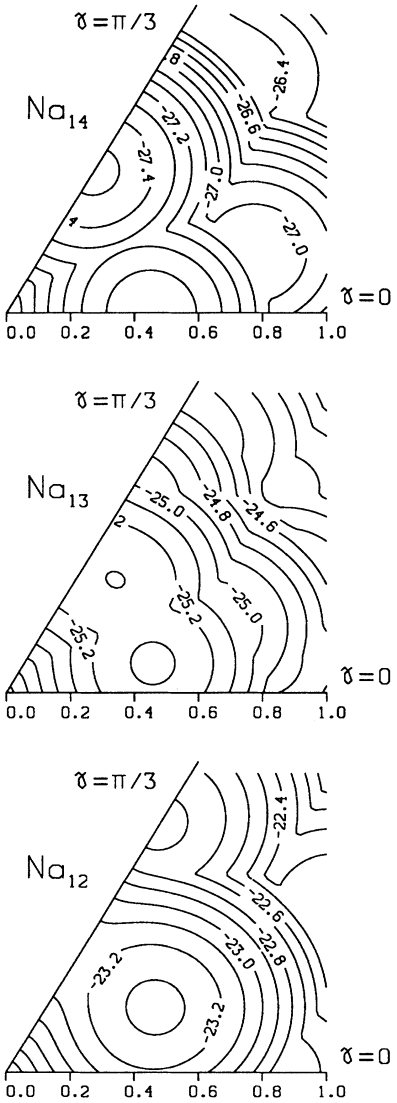

FIG. 19. PES's (according to the ellipsoidal model) for the neutral Na_{12} (bottom panel), Na_{13} (middle panel), and Na_{14} (top panel) clusters. The radius (β) and the angle γ are the Hill-Wheeler quadrupole deformation parameters. The scale of β is marked on the horizontal axes. The contour lines correspond to increments of 0.1 eV in the total energy of the clusters.

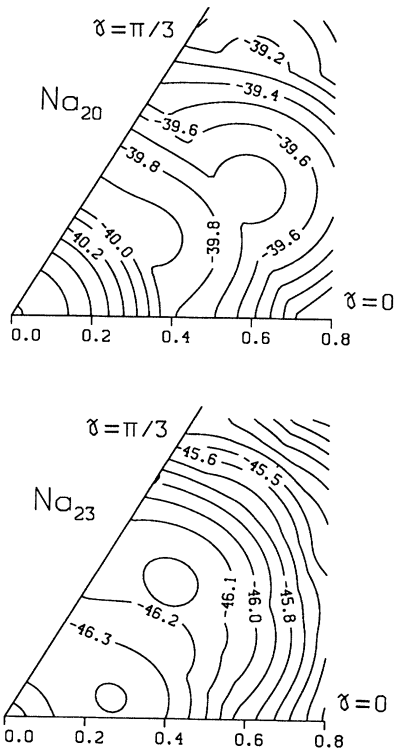

FIG. 20. PES's (according to the ellipsoidal model) for the neutral Na_{23} (bottom panel) and Na_{20} (top panel) clusters. The radius (β) and the angle γ are the Hill-Wheeler quadrupole deformation parameters. The scale of β is marked on the horizontal axes. The contour lines correspond to increments of 0.1 eV in the total energy of the clusters.

each in the case of the three axes of an ellipsoid and 2/3 and 1/3 in the case of a spheroid). These phenomenological models relate directly the resulting splitting of the plasmon line to the semiaxes [and through Eqs. (30) to the Hill-Wheeler parameters β and γ] and do not require

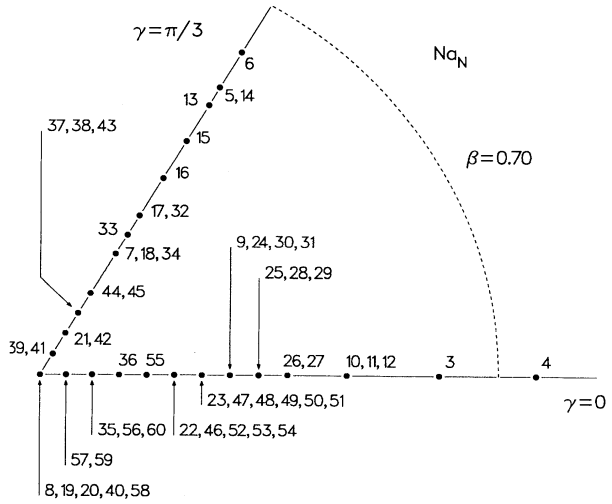

FIG. 21. The Hill-Wheeler parameters specifying the equilibrium shapes of neutral Na_N clusters according to the spheroidal model in the range $3 \leq N \leq 60$.

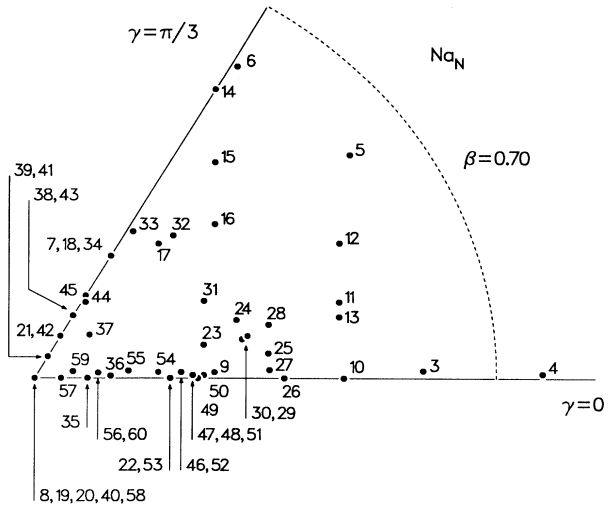

FIG. 22. The Hill-Wheeler parameters specifying the equilibrium shapes (corresponding to the global minima of the PES's) of neutral Na_N clusters according to the ellipsoidal model in the range $3 \leq N \leq 60$.

prior knowledge, or make explicit use, of the quantal structure of the clusters, as is the case with calculations based on evaluation of the total energies.

Recently, a systematic inference of shapes of $Na_N{}^+$ clusters has been carried out[27] through an attempt to draw a direct connection between shape deformations, which were presumed spheroidal, and measured photoabsorption cross sections (which were accordingly fitted with at most two Lorentz functions). Focusing on the cluster range $N = 11-21$—where our results for ground-state properties for all metal clusters studied here (especially, sodium clusters) provide a detailed description of available experimental data—we find discrepancies between the shapes predicted from our approach and those suggested in Ref. 27. For example, while in Ref. 27 prolate shapes were assigned to $Na_{14}{}^+$ and $Na_{15}{}^+$, and a spherical shape to $Na_{16}{}^+$, our results yield a triaxial, an oblate, and again a triaxial shape, respectively (note the shift by one unit in N with respect to the neutral clusters of Fig. 22). This suggests that utmost caution must be applied when shapes are inferred from experimental fits of optical absorption cross sections in conjunction with certain phenomenological models. Indeed, the difficulty in interpreting the optical cross sections is due to a strong broadening[68] of each absorption line, which can mask the plasmon splitting due to the deformation. In this context, we remark that our SE-SCM yielded results in overall agreement with the triaxial shapes inferred from the simple Clemenger-Nilsson model,[16,3] which has been used previously in the analysis of photoabsorption cross sections,[25] for clusters with $N \leq 40$. On the other hand, for clusters with N just above 40, we find oblate shapes (see Figs. 21 and 22), in correspondence with the experimental analysis of the photoabsorption experiments described in Ref. 27.

IV. CONCLUSIONS

We have adapted the semiempirical shell-correction method (familiar from nuclear physics as the Strutinsky method[30]) to calculations of total energies of open-shell metal clusters. Our method allows accurate computations for a broad range of cluster sizes which are less arduous than KS-LDA calculations, thus allowing explorations of systematic trends and confrontations between experimental observations and theoretical models for various quantities and materials.

A successful adaptation of the Strutinsky method to metal clusters was achieved by us through use of an anisotropic harmonic oscillator as the external potential mimicking the mean field acting upon the valence electrons (see Sec. II B), and generalization of the liquid-drop model to adequately describing ground-state energies of multiply charged clusters (see Sec. II A). Using our method we have calculated ground-state properties (IP's, EA's, monomer and dimer separation energies, as well as fission dissociation energies) for Na_N, K_N, and Cu_N clusters, obtaining values and trends in good agreement with experimentally measured ones.

The present paper focused on a systematic investigation of the effects of shape deformations on the energetics of metal clusters. Shape deformations in open-shell systems provide a symmetry breaking mechanism, resulting in lifting of degeneracies in the electronic spectra and lowering of the total energy of clusters. In particular, we have shown, via comparative studies, that allowing for triaxial- (ellipsoidal) shape deformations yields an overall substantial improvement in the agreement between theory and experiment, in comparison with models which are limited to consideration of spherical shapes and spheroidal deformations only. In this context, we remark that shape triaxiality provides a complete interpretation of the fine structure (including odd-even alternations) for clusters with less than 21 atoms, thus allowing for unambiguous assignments of cluster shapes in this range (see Sec. III E). For larger sizes, while the agreement obtained by us between theory and experiment is quite satisfactory, remaining discrepancies (e.g., the rather weak odd-even alternations obtained by the ellipsoidal model in comparison with the pronounced odd-even alternations in the IP's of cold Na_N and Cu_N clusters) suggest that additional shapes may come into play via the emergence of shape isomers generated either by reflection asymmetric octupole deformations or by hyperdeformed ellipsoidal shapes (work towards studying such additional shapes and their consequences is in progress[69]).

Along with underlying characteristic patterns observed in ground-state properties and those which may be obtained via ground-state total energy differences, shape deformations are portrayed also in photoabsorption data (i.e., splitting and shifting of plasmon resonances associated with anisotropy of the collective excitation spectra). Furthermore, shape deformations lead to occurrence of shape isomers (local minima of the potential energy surface in deformation space), which, depending on the conditions of the experiment (e.g., total energy content, or kinetic temperature of the clusters being investigated),

may result in multiple values for measured quantities. Indeed, inspection of such potential energy surfaces calculated by us suggests that measurements of cluster properties, and their temperature dependence, may provide information about the topology of such deformation potential energy surfaces. Finally, since the lifting of degeneracies via shape deformations modifies the level-filling scheme from that predicted by Hund's rules, we expect that such deformations would also influence the magnetic properties[70] of simple metal clusters. For example, triaxial deformations, which have been demonstrated to provide an effective mechanism for generating odd-even alternations in ground-state energetics of clusters, may also serve to quench their paramagnetism. The magnetic behavior of metal clusters, as well as thermal effects, are under investigation[69] in our laboratory.

ACKNOWLEDGMENTS

This research was supported by a grant from the U.S. Department of Energy (Grant No. FG05-86ER45234). We thank R. L. Whetten for providing us with the data on cool sodium clusters (shown in Fig. 5) prior to publication, and for useful discussions.

APPENDIX

In this appendix we present the complete matrix elements of the pseudoangular momentum operator l^2. Using the definitions (16)–(18), one first derives the operator identities,

$$l_3^2 = a_2^\dagger a_2 a_1 a_1^\dagger + a_1^\dagger a_1 a_2 a_2^\dagger - (a_1^\dagger)^2 (a_2)^2 - (a_2^\dagger)^2 (a_1)^2 , \tag{A1}$$

and likewise for l_2^2 and l_1^2 via cyclic permutation of the indices.

As a result, one has

$$\begin{aligned}\langle n_1, n_2, n_3 | l_3^2 | n_1', n_2', n_3' \rangle = {} & [n_2(n_1+1) + n_1(n_2+1)] \delta_{n_1,n_1'} \delta_{n_2,n_2'} \delta_{n_3,n_3'} \\ & - \delta_{n_3,n_3'} \delta_{n_1-2,n_1'} \delta_{n_2,n_2'-2} \sqrt{n_1(n_1-1) n_2'(n_2'-1)} \\ & - \delta_{n_3,n_3'} \delta_{n_1,n_1'-2} \delta_{n_2-2,n_2'} \sqrt{n_1'(n_1'-1) n_2(n_2-1)} .\end{aligned} \tag{A2}$$

The matrix elements of l_2^2 and l_3^2 are again determined through a cyclic permutation of the indices 1, 2, and 3.

[1] W. D. Knight, K. Clemenger, W. A. de Heer, W. A. Saunders, M. Y. Chou, and M. L. Cohen, Phys. Rev. Lett. **52**, 2141 (1984); **53**, 510(E) (1984).

[2] W. Ekardt, Phys. Rev. B **29**, 1558 (1984).

[3] For a review see W. A. de Heer, Rev. Mod. Phys. **65**, 611 (1993).

[4] For a review see W. A. de Heer, W. D. Knight, M. Y. Chou, and M. L. Cohen, in *Solid State Physics: Advances in Research and Applications*, edited by H. Ehrenreich, F. Seitz, and D. Turnbull (Academic, New York, 1987), Vol. 40, p. 93.

[5] M. Y. Chou, A. Cleland, and M. L. Cohen, Solid State Commun. **52**, 645 (1984).

[6] D. E. Beck, Solid State Commun. **49**, 381 (1984).

[7] F. Hund, *Linienspektren und Periodisches System der Elemente* (Springer, Berlin, 1927), p. 124.

[8] H. A. Jahn and E. Teller, Proc. R. Soc. London Ser. A **161**, 220 (1937).

[9] Å. Bohr and B. R. Mottelson, K. Dan. Vidensk. Selsk. Mat.-Fys. Medd. **27** (16) (1953).

[10] S. G. Nilsson, K. Dan. Vidensk. Selsk. Mat.-Fys. Medd. **29** (16) (1955).

[11] Å. Bohr and B. R. Mottelson, *Nuclear Structure* (Benjamin, Reading, MA, 1975), Vol. II.

[12] M. A. Preston and R. K. Bhaduri, *Structure of the Nucleus* (Addison-Wesley, London, 1975).

[13] Ph. J. Siemens and A.S. Jensen, *Elements of Nuclei* (Addison-Wesley, New York, 1987).

[14] K. L. Clemenger, Phys. Rev. B **32**, 1359 (1985).

[15] K. L. Clemenger, Ph.D. dissertation, University of California, Berkeley, 1985.

[16] W. A. Saunders, Ph.D. dissertation, University of California, Berkeley, 1986.

[17] J. G. Eaton, L. H. Kidder, H. W. Sarkas, K. M. McHugh, and K. H. Bowen, in *Nuclear Physics Concepts in the Study of Atomic Cluster Physics*, edited by R. Schmidt *et al.*, Lecture Notes in Physics Vol. 404 (Springer, Berlin, 1992), p. 291.

[18] W. Ekardt and Z. Penzar, Phys. Rev. B **38**, 4273 (1988).

[19] Z. Penzar and W. Ekardt, Z. Phys. D **17**, 69 (1990).

[20] We note, however, that triaxiality was incorporated in a KS-LDA calculation which was restricted in determining the optimum shapes of the following four neutral sodium clusters: Na_{10}, Na_{12}, Na_{14}, and Na_{18} [see G. Lauritsch, P.-G. Reinhard, J. Meyer, and M. Brack, Phys. Lett. A **160**, 179 (1991), and Ref. 51].

[21] D. R. Snider and R. S. Sorbello, Surf. Sci. **143**, 204 (1984).

[22] F. Iachello, E. Lipparini, and A. Ventura, in *Nuclear Physics Concepts in the Study of Atomic Cluster Physics* (Ref. 17), p. 318; F. Iachello, Nucl. Phys. **A570**, 145c (1994).

[23] M. Barranco, E. S. Hernández, R. J. Lombard, and Ll. Serra, Z. Phys. D **22**, 659 (1992).

[24] V. Bonačić-Koutecký, P. Fantucci, and J. Koutecký, Chem. Rev. **91**, 1035 (1991).

[25] K. Selby, M. Vollmer, J. Masui, V. Kresin, W. A. de Heer,

and W. D. Knight, Phys. Rev. B **40**, 5417 (1989).
[26] C. Bréchignac, Ph. Cahuzac, F. Carlier, M. de Frutos, and J. Leygnier, Chem. Phys. Lett. **190**, 42 (1992).
[27] J. Borggreen, P. Chowdhury, N. Kebaili, L. Lundsberg-Nielsen, K. Lutzenkirchen, M. B. Nielsen, J. Pedersen, and H. D. Rasmussen, Phys. Rev. B **48**, 17 507 (1993).
[28] M. Bernath, C. Yannouleas, and R. A. Broglia, Phys. Lett. A **156**, 307 (1991).
[29] W. Ekardt and Z. Penzar, Phys. Rev. B **43**, 1322 (1991).
[30] V. M. Strutinsky, Nucl. Phys. **A95**, 420 (1967); **A122**, 1 (1968).
[31] H. Koizumi, S. Sugano, and Y. Ishii, Z. Phys. D **28**, 223 (1993); M. Nakamura, Y. Ishii, A. Tamura, and S. Sugano, Phys. Rev. A **42**, 2267 (1990).
[32] C. Yannouleas, R. N. Barnett, and U. Landman, Comments At. Mol. Phys. (to be published).
[33] A. Bulgac, Phys. Rev. Lett. **71**, 4130 (1993).
[34] C. Yannouleas and U. Landman, Chem. Phys. Lett. **210**, 437 (1993).
[35] C. Yannouleas and U. Landman, Phys. Rev. B **48**, 8376 (1993).
[36] R. N. Barnett, C. Yannouleas, and U. Landman, Z. Phys. D **26**, 119 (1993).
[37] C. Yannouleas and U. Landman, Chem. Phys. Lett. **217**, 175 (1994).
[38] T. D. Newton, Can. J. Phys. **38**, 700 (1960).
[39] M. Brack, Phys. Rev. B **39**, 3533 (1989).
[40] W. A. Saunders, Phys. Rev. A **46**, 7028 (1992).
[41] Ll. Serra, F. Garcías, M. Barranco, J. Navarro, L. C. Balbás, and A. Mañanes, Phys. Rev. B **39**, 8247 (1989).
[42] In this paper, we consider clusters of monovalent elements (Na, K, and Cu). For polyvalent elements, N in Eq. (2) must be replaced by Nv, where v is the valency.
[43] For materials with high electronic densities, it is known that the usual LDA fails to provide correct values for the surface tension. Therefore, following Ref. 37, in the case of Cu clusters, we have carried out an ETF calculation using the *stabilized-jellium*-LDA (SJ-LDA) functional [for a description of the SJ-LDA energy functional, see J. P. Perdew, H. Q. Tran, and E. D. Smith, Phys. Rev. B **42**, 11 627 (1990)].
[44] I. S. Gradshteyn and I. M. Ryzhik, *Table of Integrals, Series, and Products* (Academic, New York, 1980), Chap. 8.11.
[45] R. W. Hasse and W. D. Myers, *Geometrical Relationships of Macroscopic Nuclear Physics* (Springer-Verlag, Berlin, 1988), Chap. 6.5.
[46] L. D. Landau and E. M. Lifshitz, *Electrodynamics of Continuous Media* (Pergamon Press, Oxford, 1981).
[47] The factor 3/4 arises from many-body effects, namely, from the condition that the harmonic potential is not an external potential *per se*, but an approximation to the electronic mean field (see p. 421 of Ref. 12 and Ref. 13).
[48] J. R. Nix, Annu. Rev. Nucl. Part. Sci. **22**, 65 (1972).
[49] R. K. Bhaduri and C. K. Ross, Phys. Rev. Lett. **27**, 606 (1971).
[50] The perturbation $\boldsymbol{l}^2 - \langle \boldsymbol{l}^2 \rangle_n$ in the Hamiltonian (14) influences the shell correction $\Delta E_{\rm sh}^{\rm Str}$, but not the average, $\widetilde{E}_{\rm sp}$, of the single-particle spectrum, since $U_0 = 0$ for all shells with principal quantum number n higher than the minimum number required for accommodating N_e electrons (see Ref. 11, p. 598 ff.).
[51] M. Brack, Rev. Mod. Phys. **65**, 677 (1993).
[52] W. A. Saunders, K. Clemenger, W. A. de Heer, and W. D. Knight, Phys. Rev. B **32**, 1366 (1985).
[53] M. B. Knickelbein, Chem. Phys. Lett. **192**, 129 (1992).
[54] M. L. Homer, E. C. Honea, J. L. Persson, and R. L. Whetten (unpublished).
[55] C. L. Pettiette, S. H. Yang, M. J. Craycraft, J. Conceicao, R. T. Laaksonen, O. Cheshnovsky, and R. E. Smalley, J. Chem. Phys. **88**, 5377 (1988).
[56] C. Bréchignac, Ph. Cahuzac, F. Carlier, M. de Frutos, and J. Leygnier, J. Chem. Phys. **93**, 7449 (1990).
[57] C. Bréchignac, Ph. Cahuzac, J. Leygnier, and J. Weiner, J. Chem. Phys. **90**, 1492 (1989).
[58] M. P. Iñiguez, J. A. Alonso, M. A. Aller, and L. C. Balbás, Phys. Rev. B **34**, 2152 (1986).
[59] J. M. López, J. A. Alonso, F. Garcias, and M. Barranco, Ann. Phys. (Leipzig) **1**, 270 (1992).
[60] R. N. Barnett, U. Landman, and G. Rajagopal, Phys. Rev. Lett. **67**, 3058 (1991).
[61] C. Bréchignac, Ph. Cahuzac, F. Carlier, M. de Frutos, R. N. Barnett, and U. Landman, Phys. Rev. Lett. **72**, 1636 (1994).
[62] C. Bréchignac, Ph. Cahuzac, F. Carlier, J. Leygnier, and A. Sarfati, Phys. Rev. B **44**, 11 386 (1991).
[63] Previous triaxial results from the SE-SCM approach presented in Ref. 35 were restricted to cluster sizes $N < 60$, and were derived for a simple triaxial oscillator without the $\boldsymbol{l}^2$ perturbation.
[64] D. L. Hill and J. A. Wheeler, Phys. Rev. **89**, 1102 (1953).
[65] M. B. Knickelbein and S. Yang, J. Chem. Phys. **93**, 5760 (1990).
[66] R. L. Whetten and K. E. Schriver, in *Gas Phase Inorganic Chemistry*, edited by D. H. Russell (Plenum Press, New York, 1989), p. 193.
[67] U. Röthlisberger and W. Andreoni, J. Chem. Phys. **94**, 8129 (1991).
[68] This broadening is due to thermal shape fluctuations [see C. Yannouleas, J. M. Pacheco, and R. A. Broglia, Phys. Rev. B **41**, 6088 (1990)], as well as to a temperature-independent process (referred to as Landau damping) which results from collective strength fragmentation due to couplings to incoherent particle-hole transitions [see C. Yannouleas, E. Vigezzi, and R. A. Broglia, Phys. Rev. B **47**, 9849 (1993); C. Yannouleas, Chem. Phys. Lett. **193**, 587 (1992); C. Yannouleas, M. Brack, R. A. Broglia, and P. F. Bortignon, Phys. Rev. Lett. **63**, 255 (1989), and references therein]. Microscopic calculations for the description of the latter process have been carried out primarily for closed-shell spherical clusters, with the exception of the open-shell neutral sodium clusters Na_6, Na_{10}, and Na_{12} (see Ref. 28; for a calculation regarding Na_{10}, see also Ref. 29).
[69] C. Yannouleas and U. Landman (unpublished).
[70] W. A. de Heer, Ph.D. dissertation, University of California, Berkeley, 1985.